Geomechanics and Engineering, *Vol. 28, No. 2 (2022) 135-143*
https://doi.org/10.12989/gae.2022.28.2.135

Effect of particle size on direct shear deformation of soil

Renguo Gu[1,2,3], Yingguang Fang[*2], Quan Jiang[**1], Bo Li[2] and Deluan Feng[4]

[1]*State Key Laboratory of Geomechanics and Geotechnical Engineering, Institute of Rock and Soil Mechanics, Chinese Academy of Sciences, Hubei, China*
[2]*South China University of Technology, Guangzhou, China*
[3]*State Key Laboratory of Subtropical Building Science, Guangzhou, China*
[4]*Guangdong University of Technology, Guangzhou, China*

(Received May 10, 2021, Revised June 16, 2021, Accepted September 14, 2021)

Abstract. Soils are natural granular materials whose mechanical properties differ according to the size and composition of the particles, so soils exhibit an obvious scale effect. Traditional soil mechanics is based on continuum mechanics, which can not reflect the impact of particle size on soil mechanics. On that basis, a matrix–reinforcing-particle cell model is established in which the reinforcing particles are larger-diameter sand particles and the matrix comprises smaller-diameter bentonite particles. Since these two types of particles deform differently under shear stress, a new shear-strength theory under direct shear that considers the stress concentration and bypass phenomena of the matrix is established. In order to verify the rationality of this theory, a series of direct shear tests with different reinforcing particle diameter and volume fraction ratio are carried out. Theoretical analysis and experimental results showed that the interaction among particles of differing size and composition is the basic reason for the size effect of soils. Furthermore, the stress concentration and bypass phenomena of the matrix enhance the shear strength of a soil, and the volume ratio of reinforcing particles has an obvious impact on the shear strength. In addition, the newly proposed shear-strength theory agrees well with experimental values.

Keywords: cell model; granular; shear strength; size effect; stress concentration

1. Introduction

Soil is a granular medium comprising mineral particles whose sizes range from micron clay to centimetre rubble spanning five to six orders of magnitude (Herrmann 2001, Mitchell and Soga 2005, Park *et al.* 2018). Inside soil are many intergranular interfaces whose mechanical properties differ from those of the particles (Kanchi *et al.* 2015). When soil is deformed, its particles experience uneven and discontinuous deformations such as translation, rotation, and intergranular interface slip, all of which weaken the connections between the particles and their surroundings and reduce the ability of the soil to transmit stress (Ba Ant 1999, Jiang and Liu 2003, Oda and Kazama 1998). Therefore, the mechanical properties of soil—such as the evolution characteristics, the width of the shear band, and the stress softening amplitude—differ significantly from those of traditional continuous media, with size effects associated with particle rotation and interface slip. These properties are directly related to the particle size (Morgan 1999, Morgan and Boettcher 1999, Vardoulakis and Mühlhaus 1987, Onturk *et al.* 2020), while the dilatancy characteristics and strength indicators (c and φ values) are closely related to the particle composition (Aziz 2020).

*Corresponding author, Professor.
E-mail: ygfang01@gmail.com
**Co-corresponding author, Professor
E-mail: qjiang@whrsm.ac.cn

Furthermore, many geotechnical hazards, such as landslides and debris flows, are affected by particle size and gradation (Ballesteros Canovas *et al.* 2016). Traditional soil mechanics is based on continuum mechanics, and the soil is treated as a continuous medium, so the discontinuity and the nonuniformity between the intergranular surfaces are neglected. In traditional soil mechanics, Drucker and Prager established a D-P model (Drucker and Prager 1952), and Roscoe *et al.* (1963) proposed a Cambridge model suitable for describing the deformation characteristics of normally consolidated soil and weakly over-consolidated clay, but both the D-P model and the Cambridge model are based on the elastoplastic model. That is, the traditional constitutive model does not contain scale parameters and cannot reflect the impact of particle size on soil mechanics (Nicot *et al.* 2007). Therefore, when analyzing scale problems such as shear-band evolution and debris-flow initiation, the traditional constitutive model faces difficulties (Iverson 1997, Kuhn 2005).

In order to solve the discontinuous problem of soil, many researchers have proposed some solutions.

The discrete element method (DEM) takes particles as the basic unit and considers the intergranular details of extrusion, friction, and surface slip to reveal the inherent mechanism of particle mechanical behavior (Cundall and Strack 1980, Jiang and Liu 2003). However, the research objects of this method are usually simple particle systems comprising particles at the same scale (Mishra 2003, Norouzi *et al.* 2016, Liu and Yang 2020). Its computational efficiency can be greatly compromised when large number of particles are required to model regions of

ISSN: 2005-307X (Print), 2092-6219 (Online)

(a) Soil comprising matrix–reinforcing-particle cells (b) Matrix–reinforcing-particle cell

Fig. 1 Matrix–reinforcing-particle cell element model of soil

less interest to researchers. Due to this, the application of DEM to boundary value problems has been limited (Christoph *et al.* 2019, Jia *et al.* 2020).

The discontinuous deformation analysis (DDA) cuts the research object into different block elements, and uses the principle of minimum potential energy to solve the state of each block at each time. In the DDA method, the deformation between blocks has a high degree of discontinuity (Zheng *et.al* 2016), which can better simulate discontinuity problems. However, this method is mostly used in the analysis of rock masses, and it is difficult to implement for soils with more obscure cutting surfaces, and has certain limitations.

Fang (2014a), Fang and Bo (2016) constructed a matrix–reinforcing-particle cell model that reflects the material information and particle characteristics. In this model, the soil particles are divided into matrix particles with a significant cohesive effect and reinforcing particles (RPs) with a friction effect, according to the connection characteristics and micro-heavy ratio between mineral particles. Fang (2014a) studied the particle size effect of triaxial shear based on the cell model, and the results showed that the RP size and volume ratio have a significant effect on the strength and deformation of the soil. That is, the coarse particles can enhance the strength of the soil.

Soils experience different stress and deformation states under direct shear tests and triaxial tests. In a triaxial test, the soil is subjected to both compressive and shear stresses, so the stress environment at each point in the sample is basically the same. In a direct shear test, the shear stress is applied mainly near the shear plane, so the deformation of the sample is located mainly on the shear surface. To improve the particle-size analysis method, this paper explores the size effect of soil particles under direct shear stress, analyzes the microscopic mechanism, and then establishes a theoretical analysis equation Eq. (11) for the soil cell model. At the same time, a direct shear test is carried out to verify this equation.

2. Theoretical analysis of particle size effect under direct shear

2.1 Matrix–reinforcing-particle cell element model

The scale effect exhibited by soil mechanical behavior is derived from the granularity of soil, and the size effect is strongly impacted by the components, particle sizes, and grading situations. According to experimental results (Fang and Bo 2016, Fang 2014b), the interaction between particles at different scales shows different mechanical effects and produces different macroscopic soil characteristics. Fine particles have a large specific surface area, and the particles are mainly linked by molecular bonds (van der Waals force). This cohesive effect is expressed as a macroscopic cohesive force. By contrast, coarse particles are mainly connected by contact coupling, and this elastoplastic contact is induced by gravity and external loads and behaves as a macroscopic fractional force. When coarse particles and fine particles are mixed, the cementation of fine particles to coarse particles plays a major role. Based on the mechanical effects of the interactions between different particles, particles are divided into matrix particles and RPs (Fang and Bo 2016). Matrix particles are mainly small particles, such as clay minerals, organic matter, and oxides, that are smaller than silty particles. RPs are mainly coarse particles that are larger than silty particles. When the RPs are perfectly wrapped by the matrix particles, the matrix–RP cell element model is formed by RPs and their surrounding matrix particles. In this model, the RPs are equivalent to rigid spheres, and the matrix particles are aggregated into a uniform continuous matrix medium, as shown in Fig. 1. Therefore, a cell element is the smallest unit that reflects the material information and structure information of a soil, and macroscopically the soil comprises many cells. If the volume of a cell element is V_{cell} and that of the RP in the cell is V_{r}, then the RP volume ratio is

$$\alpha = V_r / V_{cell} \tag{1}$$

If a cell element is a cube of length L and the RP diameter is d, then

$$L = (\frac{\pi}{6\alpha})^{1/3} d \tag{2}$$

To ensure that the RP does not exceed the boundary, we require $L > d$ and $\alpha < \pi/6$.

2.2 Derivation of theoretical formula

The matrix particles are assumed to be well mixed with the RPs, and the RPs are assumed to be distributed

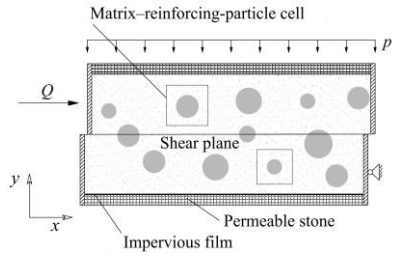

Fig. 2 Direct shear test

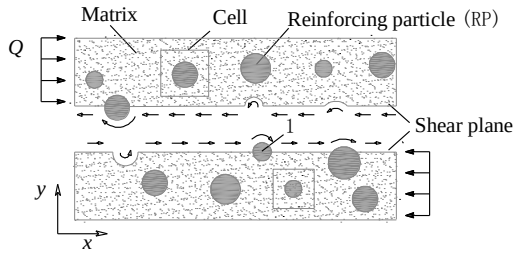

Fig. 3 Stress distribution on shear plane

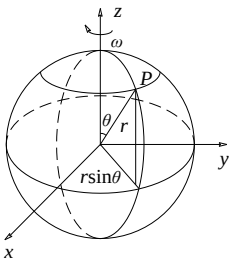

(a)

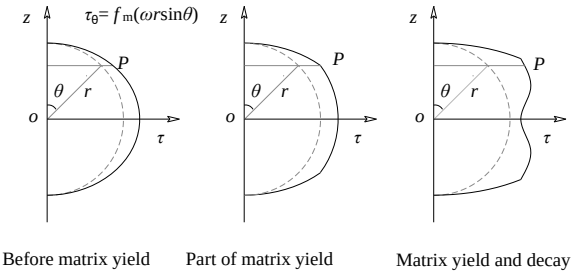

(b)

Fig. 4 Relative rotation and stress distribution of reinforcing particle (RP)

uniformly in the matrix medium. Under direct shear, the deformation is mainly shear strain and is concentrated near the shear plane, as shown in Fig. 2. The shear force on the shear plane is assumed to be approximately equal to the lateral load Q. The shear stress on the plane has two parts, namely (i) the shear stress on the matrix and (ii) the shear stress on the RPs (as shown in Fig. 3), of which the latter is derived from the relative shear displacement between the RP surface and the matrix.

It is assumed that the direction of the shear stress on the RPs is consistent with that of the shear displacement. As shown in Fig. 3, the RP labeled "1" on the shear plane is taken as the research object to analyze the shear stress on the surface of the RPs in the shear region. During the shear deformation process, because the deformation modulus of the RPs is much larger than that of the matrix, the former experience almost no deformation. Consequently, the matrix deformation must bypass the RPs, thereby causing a relative slip between them to coordinate the uneven deformation.

As shown in Fig. 4(a), the relationship between the relative shear displacement λ_θ of any point P on the RP surface and the relative stiffness rotation angle of the RP can be expressed as

$$\lambda_\theta = \omega \cdot r\sin\theta,\ 0 \le \theta \le \pi \tag{3}$$

where r is the RP radius ($r = d/2$) and θ is the angle between line OP and the axis of rotation (the z axis). The shear stress and shear displacement of the matrix are assumed to be related as

$$\tau_m = f_m(\lambda) \tag{4}$$

where τ_m is the shear stress and λ is the shear displacement of the matrix. The interface between the matrix and the RPs is assumed not to separate, so the shear stress is assumed to be continuous. That is, the shear stress on the surface of an RP is that of the corresponding point of the matrix. From Eqs. (3) and (4), the shear stress τ_θ on the RP surface can be expressed as

$$\tau_\theta = f_m(\lambda_\theta) = f_m(\omega r\sin\theta) \tag{5}$$

from which the shear stress on the surface of an RP is related to the radius of rotation ($r\sin\theta$) of the point. The distribution curves of surface shear stress for different relative stiffness rotational angles are as shown in Fig. 4(b), and the resultant shear force on the surface of an RP can be obtained by integrating the area under this curve as follows

$$F_i = \int_\Omega \tau_\theta \sin\theta \mathrm{d}S = \int_0^{2\pi}\int_0^{\pi} f_m(\omega r\sin\theta) r^2 \sin\varphi \sin\theta \mathrm{d}\varphi \mathrm{d}\theta \tag{6}$$

where the subscript i indicates RP i on the shear plane. According to the assumption that the interface between an RP and the matrix does not separate, the interfacial displacement is continuous, i.e., $\lambda_\theta = \omega r sin\theta = \lambda$. Therefore, the resultant shear force on the surface of an RP can be expressed as a function related to the shear displacement of the matrix medium

$$F_i = \frac{8r}{\omega}\int_0^{r\omega} f_m(\lambda)\frac{\lambda}{\sqrt{(r\omega)^2 - \lambda^2}}\mathrm{d}\lambda \tag{7}$$

where $f_m(\lambda)$ is the shear stress function of the matrix in the cell element.

To describe the various conditions of the relationship between the shear stress $f_m(\lambda)$ and lateral displacement λ of the pure matrix, the relationship curve is divided into three stages (as shown in Fig. 5), namely ① the linear elastic stage before yield, ② the hyperbolic stage after yield but before decay, and ③ the decay stage. The relationship can be described as follows

$$\begin{cases} f_{m1}(\lambda) = G\lambda, & 0 < \lambda \le \lambda_1 \\ f_{m2}(\lambda) = \dfrac{\lambda}{a + b\lambda}, & \lambda_1 < \lambda \le \lambda_2 \\ f_{m3}(\lambda) = \tau_s e^{-k\lambda}, & \lambda > \lambda_2 \end{cases} \tag{8}$$

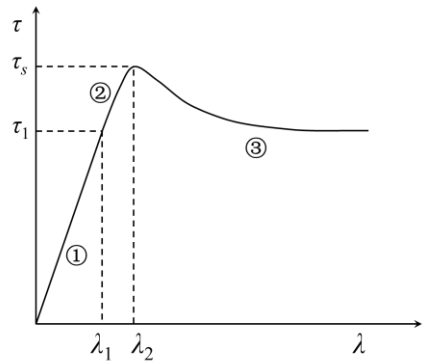

Fig. 5 Relationship between shear stress and displacement for pure matrix

where G, a, b, and k are all fitting factors that can be obtained by piecewise fitting the relationship curve between the shear stress and the shear displacement in Fig. 5. Then, combining Eqs. (7) and (8), the resultant force on the surface of an RP can be determined during the entire shearing process.

If the shear stress everywhere on the surface of an RP has reached the strength limit, then the matrix medium around the RP surface has reached the shear strength limit τ_s, as shown in Fig. 5. Then, combining Eqs. (7) and (8), the shear force limit on the RP surface can be derived as

$$F_{is}=\frac{8r}{\omega}\tau_s\int_0^{r\omega}\frac{\lambda}{\sqrt{(r\omega)^2-\lambda^2}}\mathrm{d}\lambda=8r^2\tau_s \tag{9}$$

where τ_s is the shear strength limit of the matrix. Then, combining Eqs. (7) and (8), the resultant shear force on the shear plane can be determined as

$$Q=(1-\alpha)A\tau_m+\frac{1}{2}\sum_{i=1}^{n}F_i=(1-\alpha)A\tau_m+\frac{\alpha A}{2\pi r^2}F_i \tag{10}$$

where α is the RP volume ratio, A is the area of the shear plane, $(1-\alpha)A\tau_m$ is the shear force of the matrix on the shear plane, n is the total number of RPs on the shear plane, and $\frac{1}{2}\sum_{i=1}^{n}F_i$ is the RP shear stress, in which the coefficient 1/2 is the probability average value of the surface area of the RPs on the shear plane. Therefore, the shear stress on the shear plane is given by

$$\tau_b=Q/A=(1-\alpha)\tau_m+\frac{\alpha}{2\pi r^2}F_i=(1-\alpha)f_m(\lambda_b)+\frac{\alpha}{2\pi r^2}F_i \tag{11}$$

where λ_b is the shear displacement of the sample or on the shear plane.

When the shear stress of the matrix everywhere near the RP surface reaches the strength limit, so does the cell element. Then, combining Eqs. (9)- (11), the shear strength limit of the soil sample can be expressed as

$$\tau_{bs}=Q_S/A=[(\frac{4}{\pi}-1)\alpha+1]\tau_s \tag{12}$$

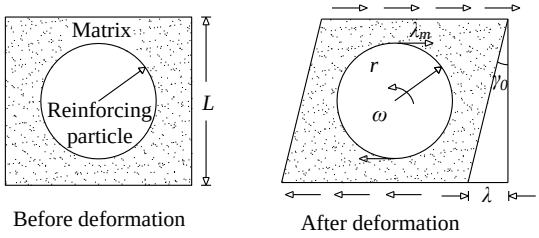

Fig. 6 Shear deformation of cell element on shear plane

Through the above analysis, the shear strength limit of the soil sample is obtained, and the relationship between shear stress and shear displacement is established. It can be seen that the shear strength is related only to the RP volume ratio and is not affected by the RP size.

3. Theoretical calculation and analysis

In this section, by analyzing (i) the RP rotation angle and (ii) the shear force on the RP surface, we determine the relationship between the relative rotation angle ω and the shear displacement λ, and the relationship between the resultant shear force F_i and the shear displacement λ. Thus, we derive a formula for calculating the shear stress τ_b on the shear plane during the entire shear process.

3.1 Relative rotation angle of reinforcing particles

When using the above equations to describe how the particle size affects the shear strength and deformation, the relationship between the RP relative rotation angle and shear displacement should be determined. The shear deformation is assumed to be concentrated on the shear plane and to decrease in the vertical direction of the shear plane as shown in Fig. 3. Then, the relationship between the shear strain and coordinate y is

$$\gamma=\gamma_0\mathrm{e}^{-\varsigma|y|} \tag{13}$$

where γ_0 is the shear strain on the shear plane and ς is the decay constant. Thus, the shear displacement is

$$\lambda=u_x\big|_{y=0}=\frac{\gamma_0}{\varsigma} \tag{14}$$

A cell element on the shear plane is selected for analysis, as shown in Fig. 6. Because the RP is much stiffer than the matrix, the shear deformation is concentrated mainly in the latter. The matrix shear strain at the RP apex position can be obtained as

$$\gamma_m=\frac{\gamma_0L^3}{L^3-\frac{4\pi r^3}{3}}=\frac{\lambda\varsigma L^3}{L^3-\frac{4\pi r^3}{3}} \tag{15}$$

Thus, the matrix shear displacement at this point can be expressed as

$$\lambda_m=\gamma_m\cdot 1=\frac{\lambda\varsigma L^3}{L^3-\frac{4\pi r^3}{3}} \tag{16}$$

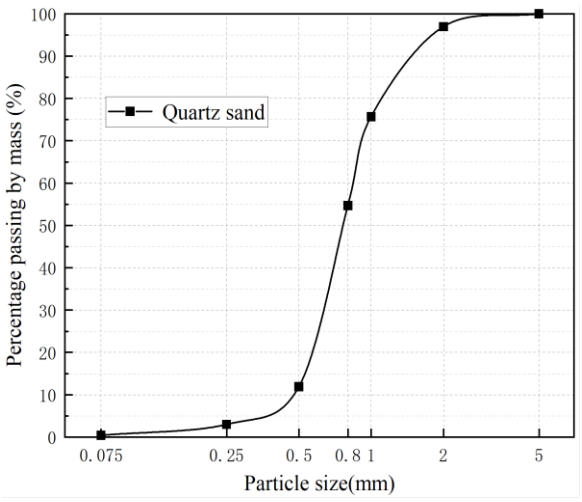

(a) The grain size distribution curve

(b) physical diagram

Fig. 7 The grain size distribution curve and physical diagram of quartz sand

The RP relative rotation angle can be described as

$$\omega = \frac{\lambda_m}{r} = \frac{\lambda \varsigma L^3}{(L^3 - \frac{4\pi r^3}{3})r} \tag{17}$$

3.2 Shear force on surface of reinforcing particle

According to Eq. (16), the shear displacement of the sample can be written as

$$\lambda_b = \frac{\lambda_m (L^3 - 4\pi r^3 / 3)}{\varsigma L^3} = \frac{\lambda_m}{\varsigma}(1 - \frac{4\pi r^3}{3L^3}) \tag{18}$$

From Figs. 4 and 5, the relationship curve of the matrix shear stress and displacement is divided into three stages (①, ②, and ③ in Fig. 5).

When the matrix at the RP apex position is yet to yield (stage ①, i.e., $\lambda_b \le = \frac{\lambda_1}{\varsigma}(1 - \frac{4\pi r^3}{3L^3})$), Eq. (7) can be expressed as

$$F_i = \frac{8r}{\omega} \int_0^{r\omega} \frac{f_{m1}(\lambda)\lambda}{\sqrt{(r\omega)^2 - \lambda^2}} \mathrm{d}\lambda \tag{19}$$

When the matrix has yielded but not yet decayed (stage ②, i.e., $\frac{\lambda_1}{\varsigma}(1 - \frac{4\pi r^3}{3L^3}) < \lambda_b \le \frac{\lambda_2}{\varsigma}(1 - \frac{4\pi r^3}{3L^3})$), Eq. (7) can be expressed as

$$F_i = \frac{8r}{\omega}\left[\int_0^{\lambda_1} \frac{f_{m1}(\lambda)\lambda}{\sqrt{(\lambda_1)^2 - \lambda^2}} \mathrm{d}\lambda + \int_{\lambda_1}^{r\omega} \frac{f_{m2}(\lambda)\lambda}{\sqrt{(r\omega)^2 - \lambda^2}} \mathrm{d}\lambda \right] \tag{20}$$

When the matrix enters the decay stage (stage ③, i.e., $\lambda_b > \frac{\lambda_2}{\varsigma}(1 - \frac{4\pi r^3}{3L^3})$), Eq. (7) can be expressed as

Table 1 Basic physical parameters of test materials

Material	Specific gravity	Liquid limit w_L [%]	Plastic limit w_s [%]	Liquidity index I_L
Bentonite	2.54	236	48	0.2
Quartz sand	2.68	—	—	—

$$F_i = \frac{8r}{\omega}\left[\int_0^{\lambda_1} \frac{f_{m1}(\lambda)\lambda}{\sqrt{(\lambda_1)^2 - \lambda^2}} \mathrm{d}\lambda + \int_{\lambda_1}^{\lambda_2} \frac{f_{m2}(\lambda)\lambda}{\sqrt{(\lambda_2)^2 - \lambda^2}} \mathrm{d}\lambda + \int_{\lambda_2}^{r\omega} \frac{f_{m3}(\lambda)\lambda}{\sqrt{(r\omega)^2 - \lambda^2}} \mathrm{d}\lambda \right] \tag{21}$$

So far, we have obtained expressions for the relative rotation angle ω Eq. (17) and the resultant shear force F_i Eqs. (19)-(21). Substituting these equations into Eq. (11) gives the relationship between the shear stress τ_b and the lateral displacement λ_b during the entire shear process.

4. Experimental results and theoretical analysis

4.1 Sample preparation

To verify the rationality of the theory of how particle size affects the direct shear deformation of soil, we performed a series of direct shear tests on samples with different RP sizes and different volume ratios. In this experiment, we used bentonite as the matrix and quartz sand as the RPs. The grain size distribution curve and physical diagram of quartz sand are shown in Fig. 7. The quartz sand is sieved to obtain three particle groups with particle sizes of 0.2~0.3, 0.5~0.6 and 0.7~0.8 mm, respectively，which are used as RPs of different particle sizes. The basic physical parameters of the materials are given in Table 1.

The matrix liquidity index was designed to be $I_L = 0.2$, and the RP volume ratio was designed to be 0, 0.067, 0.125, 0.177, and 0.223. A detailed scheme is given in Table 2.

When preparing the samples, the RPs were mixed evenly with the matrix particles with an appropriate amount of water. Then, the mixed material was molded into samples with a diameter of 61.8 mm and a height of 20 mm. The

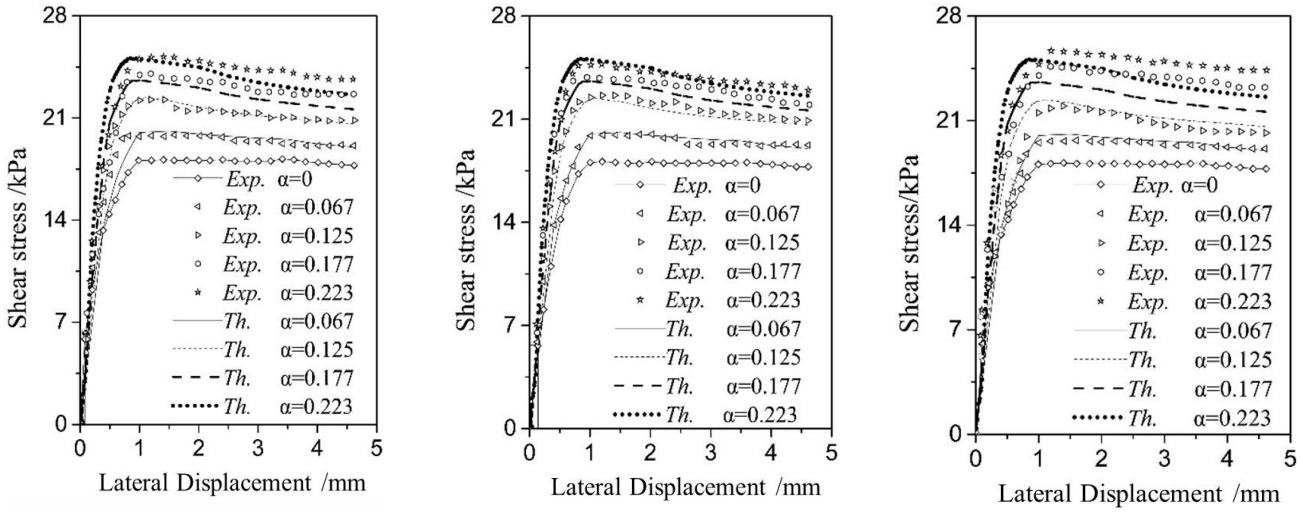

(a) d = 0.25 mm (b) d = 0.55 mm (c) d = 0.75 mm

Fig. 8 Relationship between shear stress and displacement for different volume ratios (*Th.* = theory; *Exp.* = experiment)

Table 2 Scheme of quick direct shear test

No.	I_L of matrix [%]	d [mm]	α	L [mm]
1	0.2	0.2–0.3	0, 0.067, 0.125, 0.177, 0.223	0.496, 0.403, 0.359, 0.332
2	0.2	0.5–0.6	0, 0.067, 0.125, 0.177, 0.223	1.091, 0.887, 0.790, 0.731
3	0.2	0.7–0.8	0, 0.067, 0.125, 0.177, 0.223	1.687, 1.370, 1.220, 1.130

Table 3 Parameters of equations

Parameter	Value	Parameter	Value
a	0.0182	b	0.0362
τ_s	18.084 kPa	G	31.06 kPa/mm
k	0.00129	ς	1/r mm^{-1}

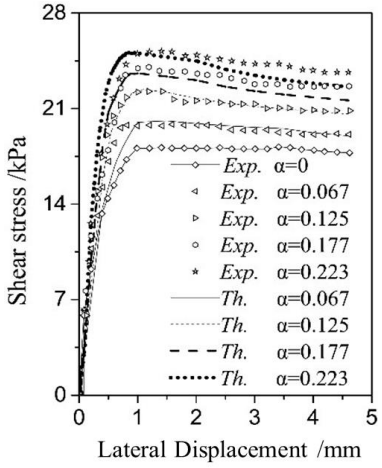

Fig. 9 Relationship between shear stress and displacement for different RP sizes

samples were subjected to vacuum evacuation and then placed where for more than 24 h. The water content of each sample after saturation was tested to ensure the same water content. For each series of samples, a set of corresponding matrix samples was prepared simultaneously to test the corresponding parameters. A direct shear test was performed on the samples at a rate of 0.8 mm/min, and the vertical pressure P was 100 kPa.

4.2 Experimental results

The equations introduced in Section 3 contain many basic parameters that can be obtained by the direct shear test of pure matrix. The parameters G, a, b, and k can be obtained by fitting the shear stress and lateral displacement curve of the pure matrix as shown in Fig. 8 (α=0) with the least square method, and τ_s represents the peak stress of the curve. The specific values of these parameters are listed in Table 3, where the decay constant is taken as $\varsigma r = 1$.

Comparisons of the theoretical calculations and the experimental results of the quick direct shear test for soil samples in various cases are shown in Figs. 8–10. Figs. 8 and 9 show that the soil shear strength is obviously enhanced with increasing RP volume ratio; however, for constant RP volume ratio, the soil shear strength is affected less by the RP size. The theoretical calculation results are consistent with the test results.

In Fig. 10, both the theoretical and experimental results showed the fact that the shear strength increases linearly with the RP volume ratio; however, for constant RP volume ratio, the shear strength is affected minimally by the RP size. The theoretical results shown in Fig. 10(b) are basically in line with the experimental results, and there are also slight deviations. The reason may be that the yield

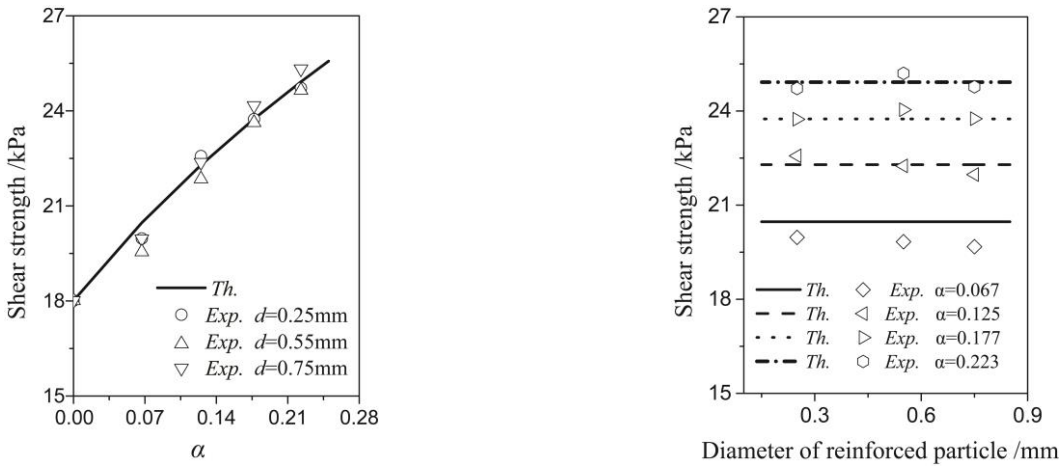

Fig. 10 Relationship between shear strength and(a) RP volume ratio and (b) RP particle size

hypothesis on the interface between the RP and the matrix is ideal in the theoretical derivation process, as shown in Fig. 4(b), which is somewhat different from the actual situation. The comparison results showed that both the lateral displacement and the shear strength exhibit an obvious size effect, indicating that the theoretical equation Eq. (11) in this paper is reasonable.

4.3 Analysis and discussion

The size effect of the soil shear deformation and strength can be explained as follows. In the soil cell model, the matrix of the cell element comprises fine particles, and the strain in the soil changes little on their scale. That is, the deformation of the matrix can be regarded as continuous, so the matrix can be considered as a continuous medium. The RPs are relatively large and rigid and are wrapped by the matrix. The coordinated deformation relationship between the matrix and the RPs concentrates strain near the interface between them, thereby changing the corresponding deformation and strength properties.

The particle size effect of direct shear deformation and strength is related mainly to the properties of the shear slip plane of the soil (upper and lower shear-box interface) and its surroundings, as shown in Eq. (13) and Fig. 3. The magnitude of the size effect can be characterized by the shear force and its degree of exertion at the interface between the RPs and matrix on the shear slip plane. Because the RPs are much stiffer than the matrix, the shear deformation is concentrated mainly in the matrix. To coordinate the differential deformation between them, the matrix must bypass the RPs, so the shear deformation path of the matrix is increased. This increased path causes the shear deformation to consume or store more energy, thereby enhancing the soil shear strength. Thus, the RPs exhibit an enhanced effect on the shear strength at the macroscopic level. When the RP volume ratio is increased, the total shear path in the soil sample increases, and thus the soil strength increases, as shown in Eq. (12).

Under the same vertical load and horizontal displacement, the larger an RP, the larger the shear stress at the interface between it and the matrix, and the larger the resultant horizontal shear force at the particle interface. Conversely, the smaller an RP, the smaller the shear stress at the interface between it and the matrix, and the smaller the degree of exertion of the shear stress, as shown in Eq. (9). When the RP volume ratio is constant, the larger an RP, the smaller the total RP surface area, that is, the fewer the RPs. Conversely, the smaller an RP, the larger the total RP surface area, that is, the more the RPs. Therefore, the final result may be that the enhanced horizontal total shear force (the horizontal total shear force of the shear stress on the matrix–RP interface) basically does not change with the RP size. However, from the perspective of the effect of RP size only, the particle size effect increases with increasing RP size, as shown in Eq. (9).

5. Conclusions

• The effect of particle size on soil strength and deformation is due to the interaction among particles of different sizes and different compositions. Fine soil particles mainly exhibit a cohesive effect, whereas coarse particles tend to be more rigid and exhibit a friction effect. Thus, when coarse particles interact with fine particles, uneven deformation and stress concentration are induced that strengthen the soil. In addition, the difference in the stiffness causes the shear deformation of the matrix to bypass the RP surface, which increases the shear deformation path of the matrix and so also the soil shear strength.

• The results of the present direct shear test show that the shear strength is obviously affected by the RP volume ratio but not by the RP size. The differences in the particle size effect between direct shear tests and triaxial tests demonstrate the intrinsic properties of the RPs in different deformation and stress states. These differences are the basic characteristics of the size effect and the performance of the intrinsic properties for the soil under different external conditions.

• The present theory based on the phenomena of shear stress concentration and the bypass of shear strain reveals the

physical mechanism of the size effect of soil samples under a quick direct shear test. At the same time, the results of this theory agree well with the test results.

Data availability statement

All data, models, and code generated and/or used during this study are available from the corresponding author by request.

Acknowledgments

This work was supported by the Open Research Fund of the State Key Laboratory of Geomechanics and Geotechnical Engineering, Institute of Rock and Soil Mechanics, Chinese Academy of Sciences (Grant No. Z018019), the State Key Laboratory of Subtropical Building Science, South China University of Technology (Grant No. 2017KB16), and the National Key Scientific Instruments and Equipment Development Projects of China (Grant No. 41827807).

References

Aziz, M. (2020), "Using grain size to predict engineering properties of natural sands in Pakistan", *Geomech. Eng*., **22**(2), 165-171. https://doi.org/10.12989/gae.2020.22.2.165.

Ba Ant, Z.P. (1999), "Size effect on structural strength: a review", *Arch. Appl. Mech.*, **69**(9-10), 703-725. https://doi.org/10.1007/s004190050252.

Ballesteros Canovas, J.A., Stoffel, M., Corona, C., Schraml, K., Gobiet, A., Tani, S., Sinabell, F., Fuchs, S. and Kaitna, R. (2016), "Debris-flow risk analysis in a managed torrent based on a stochastic life-cycle performance", *Sci. Total Environ.*, **557-558**, 142-153. https://doi.org/10.1016/j.scitotenv.2016.03.036.

Christoph, M., Weissbach, R., Weinberg, J., Wall, W.A. and Hart, A.J. (2019), "Modeling and characterization of cohesion in fine metal powders with a focus on additive manufacturing process simulations", *Powder Technol.*, **343**, 855-866. https://doi.org/10.1016/j.powtec.2018.11.072.

Cundall, P.A. and Strack, O.D.L. (1980), "Discussion: A discrete numerical model for granular assemblies", *Géotechnique*, **30**(3), 331-336. https://doi.org/10.1680/geot.1980.30.3.331.

Drucker, D.C. and Prager, W. (1952), "Soil mechanics and plastic analysis or limit design", *Q. Appl. Math.*, **10**(2), 157-165. https://doi.org/10.1090/qam/48291.

Fang, Y. (2014a), "Theoretical and experimental investigation on size effect characteristic of strength and deformation of soil", *Yantu Lixue/Rock Soil Mech.*, **35**(1), 41-47. https://doi.org/10.7498/aps.63.034502.

Fang, Y. (2014b), "Shear test and physical mechanism analysis on size effect of granular media", *Wuli Xuebao/Acta Physica Sinica*, **63**(3), 274-283. https://doi.org/10.7498/aps.63.034502.

Fang, Y.G. and Bo, L. (2016), "Multiscale problems and analysis of soil mechanics", *Mech. Mater.*, **103**, 55-67. https://doi.org/10.1016/j.mechmat.2016.09.003.

Herrmann, H.J. (2001), "Granular matter", *Proceedings of the 10th International Summer School on Fundamental Problems in Statistical Physics* Altenberg Germany, August.

Iverson, R.M. (1997), "The physics of debris flows", *Rev. Geophys.*, **35**(3), 245-296. https://doi.org/10.1029/97RG00426.

Jia, M.C., Liu, B., Xue, J.F. and Ma, G.Q. (2020), "Coupled three-dimensional discrete element–finite difference simulation of dynamic compaction", *Acta Geotech*. https://doi.org/10.1007/s11440-020-01055-y.

Jiang, Y. and Liu, M. (2003), "Granular elasticity without the Coulomb condition", *Phys. Rev. Lett.*, **91**(14), 144301. https://doi.org/10.1103/PhysRevLett.91.144301.

Kanchi, G.M., Neeraja, V.S. and Babu, G.L.S. (2015), "Effect of anisotropy of fibers on the stress-strain response of fiber-reinforced soil", *Int. J. Geomech.*, **15**(1), 06014016. https://doi.org/10.1061/(ASCE)GM.1943-5622.0000392.

Kuhn, M.R. (2005), "Are granular materials simple? An experimental study of strain gradient effects and localization", *Mech. Mater.*, **37**(5), 607-627. https://doi.org/10.1016/j.mechmat.2004.05.001.

Liu, D. and Yang, J. (2020), "Efficient flexible boundary algorithms for DEM simulations of biaxial and triaxial tests", *Geomech. Eng*., **23**(3), 189-206. https://doi.org/10.12989/gae.2020.23.3.189.

Mishra, B.K. (2003), "A review of computer simulation of tumbling mills by the discrete element method: Part I—contact mechanics", *Int. J. Miner. Process.*, **71**(1-4), 73-93. https://doi.org/10.1016/S0301-7516(03)00031-0.

Mitchell, J.K. and Soga, K. (2005), *Fundamentals of Soil Behavior*, (3rd Edition), John Wiley and Sons Inc., New York. NY, USA.

Morgan, J.K. (1999), "Numerical simulations of granular shear zones using the distinct element method - 2. Effects of particle size distribution and interparticle friction on mechanical behavior", *J. Geophys. Res. Solid Earth*, **104**(2), 2721-2732. https://doi.org/10.1029/1998JB900055.

Morgan, J.K. and Boettcher, M.S. (1999), "Numerical simulations of granular shear zones using the distinct element method: 1. Shear zone kinematics and the micromechanics of localization", *J. Geophys. Res. Solid Earth*, **104**(2), 2703-2719. https://doi.org/10.1029/1998JB900056

Nicot, F.O., Sibille, L., Donze, F. and Darve, F. (2007), "From microscopic to macroscopic second-order work in granular assemblies", *Mech. Mater.*, **39**(7), 664-684. https://doi.org/10.1016/j.mechmat.2006.10.003.

Norouzi, H.R., Zarghami, R., Sotudeh-Gharebagh, R. and Mostoufi, N. (2016), *Coupled CFD-DEM Modeling: Formulation, Implementation and Application to Multiphase Flows*. John Wiley and Sons Inc., New York. NY, USA.

Oda, M. and Kazama, H. (1998), "Microstructure of shear bands and its relation to the mechanisms of dilatancy and failure of dense granular soils", *Géotechnique*, **48**(4), 465-481. https://doi.org/10.1680/geot.1998.48.4.465.

Onturk, K., Bol, E., Ozocak, A. and Edil, T.B. (2020), "Effect of grain size on the shear strength of unsaturated silty soils", *Geomech. Eng*., **23(**4), 301-311. https://doi.org/10.12989/GAE.2020.23.4.301.

Park, T.W., Kim, H.J., Tanvir, M.T., Lee, J.B. and Moon, S.G. (2018), "Influence of coarse particles on the physical properties and quick undrained shear strength of fine-grained soils", *Geomech. Eng*., **14**(1), 99-105. https://doi.org/10.12989/gae.2018.14.1.099

Roscoe, K.H., Schofield, A.N. and Thurairajah, A., (1963), "Yielding of clays in state wetter than critical",*Geotechnique*, **13**(3), 21-40. https://doi.org/10.1680/geot.1963.13.3.211.

Vardoulakis, I. and Mühlhaus, H.B. (1987), "The thickness of shear bands in granular materials", *Géotechnique*, **37**(3), 271-283. https://doi.org/10.1680/geot.1987.37.3.271.

Zheng, H., Zhang, P. and Du, X. (2016), "Dual form of discontinuous deformation analysis", *Comput. Method. Appl. M*., **305**, 196-216, https://doi.org/10.1016/j.cma.2016.03.008.

CC

Notation

The following symbols are used in this paper:

a	one of two fitting factors for segment ② of relationship curve in Fig. 5
A	area of shear plane
b	other fitting factor for segment ② of relationship curve in Fig. 5
d	diameter of RP
G	fitting factor for segment ① of relationship curve in Fig. 5
I_L	liquidity index of sample
k	fitting factor for segment ③ of relationship curve in Fig. 5
L	length of cell element
n	total number of RPs on shear plane
V_{cell}	volume of cell element
V_r	volume of RP
r	radius of RP
F_i	resultant shear force on surface of RP *i* on shear plane
F_{is}	shear force limit on surface of RP
Q	resultant lateral force on shear plane
Q_S	shear stress limit on shear plane
γ	shear strain of pure matrix medium
γ_m	shear strain of matrix
γ_0	shear strain on shear plane
τ_1	shear stress of matrix at end of stage ① in Fig. 5
τ_2	shear stress of matrix at end of stage ② in Fig. 5
τ_s	shear strength limit of matrix in Fig. 5
τ_b	shear stress on shear plane
τ_θ	shear stress on surface of RP
τ_m	shear stress of matrix in cell element
τ_{bs}	shear strength limit
θ	angle between line *OP* and axis of rotation (*z* axis)
α	volume ratio of RP
λ	lateral displacement of sample
λ_m	shear displacement of matrix at RP apex position
λ_1	λ_m value at end of stage ① in Fig. 5
λ_2	λ_m value at end of stage ② in Fig. 5
λ_θ	relative shear displacement of any point on RP surface
ω	relative stiffness rotation angle of RP
ς	decay constant of shear strain near shear plane
$f_m(\lambda)$	shear stress function of matrix in cell element